Open Access Full Text Article

ORIGINAL RESEARCH

3D-printed scaffolds of mesoporous bioglass/gliadin/polycaprolactone ternary composite for enhancement of compressive strength, degradability, cell responses and new bone tissue ingrowth

Yiqun Zhang[1]
Wei Yu[1]
Zhaoyu Ba[2]
Shusen Cui[1]
Jie Wei[3]
Hong Li[4]

[1]Department of Hand Surgery, China-Japan Union Hospital, Jilin University, Changchun 130033, China; [2]Department of Spinal Surgery, Shanghai East Hospital, Tongji University School of Medicine, Shanghai 200120, China; [3]Key Laboratory for Ultrafine Materials of Ministry of Education, East China University of Science and Technology, Shanghai 200237, China; [4]College of Physical Science and Technology, Sichuan University, Chengdu 610041, China

Correspondence: Zhaoyu Ba
Department of Spinal Surgery, Shanghai East Hospital, Tongji University School of Medicine, 150th, Jimo Road, Shanghai 200120, China
Email greatspine@163.com

Shusen Cui
Department of Hand Surgery, China-Japan Union Hospital, Jilin University, 126th, Xiantai Street, Changchun 130033, China
Email sscui916@126.com

Background: Due to the increasing number of patients with bone defects, bone nonunion and osteomyelitis, tumor and congenital diseases, bone repair has become an urgent problem to be solved.
Methods: In this study, the 3D-printed scaffolds of ternary composites containing mesoporous bioglass fibers of magnesium calcium silicate (mMCS), gliadin (GA) and polycaprolactone (PCL) were fabricated using a 3D Bioprinter.
Results: The compressive strength and in vitro degradability of the mMCS/GA/PCL composites (MGPC) scaffolds were improved with the increase of mMCS content. In addition, the attachment and proliferation of MC3T3-E1 cells on the scaffolds were significantly promoted with the increase of mMCS content. Moreover, the cells with normal phenotype attached and spread well on the scaffolds surfaces, indicating good cytocompatibility. The scaffolds were implanted into the femur defects of rabbits, and the results demonstrated that the scaffold containing mMCS stimulated new bone formation and ingrowth into the scaffolds through scaffolds degradation in vivo. Moreover, the expression of type I collagen into scaffolds was enhanced with the increase of mMCS content.
Conclusion: The 3D-printed MGPC scaffold with controllable architecture, good biocompatibility, high compressive strength, proper degradability and excellent in vivo osteogenesis has great potential for bone regeneration.
Keywords: ternary composites, polymer-based composite, biocompatibility, cytocompatibility, osteogenesis

Introduction

Scaffolds for bone regeneration are designed to act as a 3D support structure to the surrounding tissues with advantageous characteristics, including porous structure that promotes cell–biomaterial interactions (cells adhesion, growth, and migration); interconnected pores to facilitate transport of mass, nutrients, and regulatory factors to allow cell survival, proliferation, and differentiation; controlled degradation, etc.[1,2] Over the past few decades, the design, characterization, and biological evaluation of inorganic/organic composite scaffolds containing bioactive materials and degradable polymers with the great potential for applications in regenerative medicine have been studied.[3,4] The great research efforts for designing ideal composite scaffolds for repair and regeneration of damaged/diseased tissues have revealed the promise of polymer-based composites due to the ability to mimic the structural property of native bone tissues.[5]

Polymer-based composite scaffolds have been fabricated with specific pore size and morphology, porosity, and pore interconnection by means of different technologies including foam replica method, freeze-drying, gas foaming, solvent casting and particulate-leaching, phase separation and electrospinning, etc.[6–8] These methods are often inexpensive, simple to design, and flexible to optimize or modulate physical–chemical properties.[6–8] However, the disadvantages of these methods are that they cannot efficiently control the porous structures of the scaffolds, such as pore morphology, pore size, porosity, and pore interconnectivity.[6–8] Recently, 3D-printing technology for the production of composite scaffold has attracted a great deal of attention due to the ability to prepare the scaffolds with controllable porous structure (eg, porosity, pore size, pore morphology, and pore interconnection), which benefits cell ingrowth and nutrient delivery.[9,10] Biodegradable polymer of polycaprolactone (PCL) with good biocompatibility has been extensively studied and applied in the field of tissue engineering and regeneration medicine.[11] Nevertheless, the disadvantages of PCL (eg, lack of bioactivity and slow degradation rate) as bone repair material might lead to the low bone regeneration ability in vivo. In order to improve the bioactivity and degradability of PCL, bioactive inorganic materials, such as hydroxyapatite, calcium phosphate, bioglass, and calcium silicate, have been incorporated into PCL to prepare bioactive composites. Moreover, natural polymers (such as, zein, starch, and gelatin) have been incorporated into PCL to prepare polymer-based composites with improved bioperformances (eg, degradability).[12] Gliadin (GA) materials, as one of the natural polymers, with excellent mechanical properties and degradability have been produced from wheat protein for potential use in tissue culture and other medical applications.[13] Moreover, GA has been shown to promote the attachment and proliferation of bovine turbinate fibroblasts.[14]

Over the past few decades, mesoporous bioactive glasses (MBGs) with highly ordered nanoporous channel, large surface area, and high pore volume exhibited improved degradability and bioactivity compared with conventional bioglasses, and therefore, have been proposed for applications in regeneration medicine.[15] As one of the MBGs, the mesoporous magnesium calcium silicate (mMCS) bioglass as bone repair biomaterial was previously developed by our laboratory and others, which exhibited superior in vitro bioactivity, cytocompatibility, and in vivo osteogenesis when compared with non-mMCS.[16,17] Natural polymers are appealing owing to their fast degradation rates, whereas bioactive

inorganic materials offer the required osteoconductivity and biocompatibility features. Therefore, in this study, mMCS fibers were fabricated, and novel 3D-printed scaffolds of ternary composites including mMCS, GA, and PCL (MGPC) were prepared. Moreover, the compressive strength, in vitro degradability, and cell responses to the MGPC scaffolds were evaluated, and the in vivo osteogenesis and degradability of MGPC scaffold were further investigated by implanting the scaffolds in the femur defects of rabbits.

Materials and methods
Preparation of mMCS fibers
The mMCS fibers were prepared using sol–gel method. Briefly, deionized water and nitric acid (2 M) were mixed in a volume ratio of 6:1. Polyethylene oxide–polypropylene oxide–polyethylene oxide (P123) was used as the pore-foaming agent and dissolved into the mixed solution containing deionized water and nitric acid. Afterward, tetraethyl orthosilicate (TEOS) and triethyl phosphate (TEP) were added into the solution successively and stirred at room temperature for 1 hour (the molar ratio of TEOS/TEP solution was 2.5 M). Then, calcium nitrate tetrahydrate ($Ca(NO_3)_2 \cdot 4H_2O$) and magnesium nitrate ($Mg(NO_3)_2$) were added into the resultant solution and stirred at 50°C until the entire nitrate salt was totally dissolved. The obtained sol samples were tightly sealed and maintained at 37°C for 7 days until the gelation was completed. Afterward, all of the samples were dried at 70°C. After completely dried, the samples were calcined at 700°C for 5 hours with the heating rate of 1°C/min. All chemicals were purchased from Sigma-Aldrich (St Louis, MO, USA) without further purification.

The mMCS fibers were characterized by transmission electron microscopy (TEM, JEM-2100F; JEOL Ltd., Tokyo, Japan), field emission scanning electron microscopy (FE-SEM, S-4800; Hitachi, Tokyo, Japan) equipped with energy dispersive spectrometry (EDS), and small angle and wide angle powder X-ray diffraction (XRD, D/MAX2550VB/PC; Rigaku Co., Tokyo, Japan). In addition, N_2 adsorption–desorption isotherms of mMCS were obtained by a Tristar II 3020 (Micromeritics, Norcross, GA, USA), and Brunauer–Emmett–Teller (BET) and Barrett–Joyner–Halenda (BJH) were used to determine specific surface area and inner pore size distribution of mMCS.

Preparation and characterization of MGPC scaffolds
PCL (Mn =80,000, Tm =60°C, and ρ=1.145 g/cm³) was purchased from Sigma-Aldrich. GA with biochemical purity

was obtained from CpG Biotech Co., Ltd. (Shanghai, China). PCL (1 g) was dissolved in chloroform (20 mL) at 80°C to form a uniform solution with a concentration of 5% (w/v), followed by the incorporation of mMCS powders and GA solution (dissolved by ethanol) into the PCL solution. Then the suspension of mMCS/GA/PCL was immediately dispersed with continuous stirring and ultrasonication at room temperature. Finally, the mMCS/GA/PCL (15:15:70, w/w/w, 15 MGPC) and mMCS/GA/PCL (30:15:55, w/w/w, 30 MGPC) ternary composites were prepared (Table 1). The GA/PCL composite (15:85, w/w, GPC) was prepared by the same method as controls.

The 3D-printed scaffolds were prepared using a 3D Bioprinter (Qingdao Unique Co., Ltd., Qingdao, China) at a temperature of 130°C, and the feeding rate was 100 mm/min. Briefly, the composite powders (GPC, 15 MGPC, and 30 MGPC) were heated up to 130°C for 30 minutes, and screw-extruded through a metal nozzle of gage 2 (inner diameter of 0.33 mm). The x–y movement of the motorized stage and z-movement of the nozzle were controlled by a computer to produce three-dimensional scaffolds. The GPC, 15 MGPC, and 30 MGPC scaffolds (Φ 12×2 mm, Φ 5×5 mm) were fabricated at a line width of 500 μm, pore size of 500 μm, and line height of 500 μm.

All the samples were characterized by SEM (S-4800; Hitachi). The compressive strength of the porous samples of PCL, GPC, 15 MGPC, and 30 MGPC was determined using a mechanical testing machine (HY-0230; Hengyijingmiyiqi Co., Ltd., Shanghai, China). W1 was the dry weight of the samples, W2 was the wet weight of the samples, and W3 was the weight of the samples suspended in water. The porosity of the samples was determined by using Archimedes method:

$$\text{Porosity (\%)} = \frac{(W2 - W1)}{(W2 - W3)} \times 100.$$

Degradability of scaffolds in Tris–HCl

The in vitro degradation properties of GPC, 15 MGPC, and 30 MGPC were determined by measuring the weight change of

Table 1 Compositions of scaffolds prepared by 3D-printing method

Samples	GPC	15 MGPC	30 MGPC
GA	15 w%	15 w%	15 w%
mMCS	0	15 w%	30 w%
PCL	85 w%	70 w%	55 w%

Abbreviations: GA, gliadin; MGPC, mMCS/GA/PCL composites; mMCS, mesoporous magnesium calcium silicate; PCL, polycaprolactone.

the samples after immersed into aminomethane hydrochloride (Tris–HCl) for different times. The weight change of the samples before and after soaking into Tris–HCl solution for 2 weeks was monitored by the electronic analytical balance. The W0 was the sample weight before soaking and Wn was sample weight after soaking for different times, and the percentage of weight change was calculated according to the following equation:

$$\text{Weight change (\%)} = \frac{W0 - Wn}{W0} \times 100.$$

The surface morphology of samples immersed in Tris–HCl solution for 1 week was observed using SEM.

Cells responses to scaffolds

The GPC, 15 MGPC, and 30 MGPC scaffolds were sterilized by Co60-g ray in advance at Shanghai Heming Radiation Technology Co. Ltd., which were used to evaluate the cell responses in vitro and implantation in vivo.

Murine MC3T3-E1 cells were purchased from Sigma-Aldrich. According to the manufacturer's specifications, the cells were cultured in media composed of alpha-modified minimum essential medium (α-MEM; Gibco, Thermo-Fisher Scientific, Waltham, MA, USA) supplemented with 10% fetal bovine serum (Gemini, Calabasas, CA, USA) and 1% penicillin/streptomycin (Gibco, ThermoFisher Scientific) at 37°C in a 5% CO_2 incubator. The MC3T3-E1 cells were seeded onto the scaffolds at a density of 5×10^4 cells per scaffold. The media were replaced every 2 days. GPC, 15 MGPC, and 30 MGPC samples (Φ 12×2 mm) were used for the evaluation of MC3T3-E1 cells responses.

Cell attachment ratio

The samples of GPC, 15 MGPC, and 30 MGPC (Φ 12×2 mm) were placed into a 24-well culture plate and the MC3T3-E1 cells suspension of 5×10^5 mL^{-1} cell density was seeded on samples. After cultured for 6, 12, and 24 hours, the samples were taken out and carefully washed three times with PBS to remove the unattached MC3T3-E1 cells. Then the samples were transferred into a new 24-well culture plate with 0.3 mL pancreatic enzyme. After 3 minutes of digestion by pancreatic enzyme, the α-MEM was added to terminate the pancreatic enzyme digest. At last, the cell suspension was obtained for detecting the number of the adhered MC3T3-E1 cells. The cell adhesion ratio (Ln) was calculated by the following equation:

$$Ln = \frac{Sn}{Jn} \times \frac{Sp}{Ss} \times 100\%.$$

where Sn was the number of the adhered MC3T3-E1 cells, Jn was the number of the seeded MC3T3-E1 cells, Ss was the area of the bottom of the 24-well culture plate, and Sp was the area of the sample surface.

Cell morphology

The morphology of MC3T3-E1 cells cultured on the samples (GPC, 15 MGPC, and 30 MGPC) at a density of 5×10^4 cells per scaffold was observed using the FE-SEM after 3 days culture. All samples were washed with PBS buffer, fixed in 2.5% glutaraldehyde solution for 30 minutes, and then dehydrated with graded ethanol solutions (25%, 50%, 75%, 95%, and 100%, 15 minutes each concentration). The cell morphology on the dehydrated samples was investigated by FE-SEM after sputter coating.

Cell proliferation

Cell Counting Kit-8 (CCK-8) assay was employed to quantitatively assess the level of cell proliferation at 1, 3, and 5 days. The samples of GPC, 15 MGPC, and 30 MGPC (Φ 12×2 mm) were placed into the wells of a 24-well plate (Costar; Corning Incorporated, Corning, NY, USA). The MC3T3-E1 cells were digested with 0.25% trypsin (Sigma-Aldrich), and resuspended with culture medium, counted using a cell viability analyzer (Vi-cell XR; Beckman Coulter Inc., Brea, CA, USA), and seeded in each well at a density of $3 \times 10^4 / cm^2$. The culture plates were incubated at 37°C in a humidified atmosphere of 5% CO_2. At each time point, the samples were gently rinsed three times with PBS (pH=7.4) to remove the unattached cells and transferred to a new 24-well plate. A total of 50 µL of CCK-8 solution (Dojindo Molecular Technologies Inc., Kumamoto, Japan) was added into each well and incubated for 3 hours. After this incubation, 100 µL of the supernatant was transferred into a 96-well plate and read at 450 nm using a microplate reader (Synergy HT; Biotek, Winooski, VT, USA) with 620 nm as the reference wavelength.

Scaffolds implanted into the femoral defects of rabbits

Animals and surgical procedures

Twenty-seven female rabbits (3 months old, 3–4 kg) were used. All experimental procedures were approved by the Animal Experiment and Care Committee of Ninth People's Hospital affiliated to Shanghai Jiao Tong University School of Medicine. The National Institutes of Health guidelines for the care and use of laboratory animals (NIH publication no. 85–23 Rev. 1985) were observed. The 27 rabbits were randomly assigned to three groups (n=9 each) for

implantation of different types of scaffolds. Surgery was conducted under general anesthesia and performed in sterile conditions. According to the method described, the right femur of each rabbit was exposed and one defect (Φ 5 mm) was drilled in the distal part of the femur. The bone cavities were carefully washed to eliminate bone debris and dried with gauze. Cylindrical scaffold samples (Φ 5×5 mm) were implanted into the defects in the rabbit femora. After implanted for 1, 2, and 3 months, animals were sacrificed and the femur bone of the rabbits was harvested and fixed in 10% formalin. The fixed samples were washed with PBS and photographed, and then all samples were analyzed by histological section.

Histological analysis

The lower limbs (1, 2, and 3 months) of each rabbit were harvested and dissected so that they were free of soft tissue. Sections containing the defect area were cut with a slow-speed saw. The specimens were fixed with a 10% neutral formalin solution for 48 hours. Each specimen was demineralized for H&E staining. The specimens were decalcified with 10% EDTA, and embedded in paraffin followed with H&E staining. The quantity of new bone area ratio and material residual (MR) ratio were assessed using Image-Pro Plus 6.0 software (Media Cybernetics, Rockville, MD, USA) according to the following equation:

$$\text{New bone area ratio (\%)} = \frac{\text{New bone area (cm}^2)}{\text{All area-blank (cm}^2)} \times 100;$$

$$\text{Material residual ratio (\%)} = \frac{\text{Material residual (cm}^2)}{\text{All area-blank (cm}^2)} \times 100.$$

Three microscopy images were obtained from three randomly selected areas for each sample and then histomorphometrically evaluated using Image-Pro Plus.

Immunohistochemical analysis

For immunohistochemical assessment, the expression of type I collagen, which is expressed in the osteoid matrix, was detected according to the following procedure. Following the process of deparaffinating, rehydrating, and washing with PBS, the sections were incubated with 0.3% hydrogen peroxide for 20 minutes followed by incubation with BSA for 30 minutes. Then the sections were incubated with the primary antibody for type I collagen (1:100; Boster SA2005; Boster Co., Wuhan, China) for 2 hours at 37°C. In accordance

with the manufacturer's protocol, the sections were incubated using the SP 9000 immunohistochemical kit (Zhongshan Biotechnology Co., Ltd., Zhongshan, China) and visualized by 3,3-diaminobenzidine tetrahydrochloride (Zhongshan Biotechnology Co., Ltd.). Finally, the images of all stained sections were captured with an Olympus DP72 microscope. To compare the difference of bone regeneration in three scaffolds, a quantitative analysis of type I collagen positive area was performed by counting positive pixel areas using the built-in tools in Adobe Photoshop CS6 (Adobe Systems, San Jose, CA, USA) according to the following equation:

$$\text{Positive expression (\%)} = \frac{\text{Positive expression area (cm}^2)}{\text{All area-blank (cm}^2)} \times 100.$$

Statistical analysis

All data analysis was performed using SPSS 17.0 software, and statistically significant values were adopted as $P<0.05$. For the proliferation of MC3T3-E1 mean and SD were analyzed using Student's t-test, and other data were compared using one-way ANOVA, followed by the post hoc Student–Newman–Keuls test.

Results
Characterization of mMCS fibers

Figure 1A shows the SEM micrograph of mMCS fibers. The mMCS fibers possessed the size of around 1 µm in diameter and around 5 µm in length. Figure 1B shows the TEM micrograph of the surface morphology of a single mMCS fiber. The well-ordered nanoporous channels were found inside the mMCS fiber. Figure 1C presents the N_2 adsorption–desorption isotherms of mMCS; it was a typical Type IV isotherm pattern, revealing that the mMCS fibers possessed nanoporous structure. The distribution of nanopores of mMCS was narrow, and the nanopore size was around 4 nm (Figure 1D). The specific surface area and pore volume of mMCS fibers were 678.5 m^2/g and 0.43 m^3/g, respectively. Figure 1E shows the small angle XRD of mMCS. It was found that a diffraction peak appeared in the low angle, indicating an aligned mesoporous structure. The wide-angle XRD pattern of mMCS is shown in Figure 1F. It was found that the mMCS exhibited a bread peak, illustrating an amorphous structure. Figure 1G shows the EDS of mMCS, and the peaks of Ca, Mg, and Si were found.

Characterization of scaffolds

The porosity and compressive strength of PCL, GPC, 15 MGPC, and 30 MGPC scaffolds are shown in Table 2. It was found that porosity of PCL, GPC, 15 MGPC, and 30 MGPC scaffolds was 79.3%, 78.1%, 77.6%, and 78.4%, respectively, and no obvious difference was found. The compressive strength of PCL, GPC, 15 MGPC, and 30 MGPC scaffolds was 8.6, 8.4, 10.5, and 12.1 MPa, respectively. As the content of mMCS grew, the compressive strength was improved. The SEM micrographs of surface morphology of GPC, 15 MGPC, and 30 MGPC scaffolds are shown in Figure 2. It can be seen that the three kinds of scaffolds possessed well interconnected macropores with the pore sizes of about 300 µm. Moreover, the surfaces of both 30 MGPC and 15 MGPC scaffolds containing mMCS became rough while GPC showed smooth surface without mMCS.

Degradation of scaffolds in Tris–HCl solution

Figure 3A–D shows the SEM micrographs of surface morphology of 30 MGPC, 15 MGPC, GPC, and PCL scaffolds after immersed in Tris–HCl solution for 2 weeks. It was found that the surfaces of all scaffolds showed microporous structure due to the degradation of the scaffolds (mMCS and GA first degradation, which was faster than PCL). Moreover, the 30 MGPC scaffolds exhibited more micropores than 15 MGPC and GPC scaffolds. However, PCL scaffold showed a few micropores on its surface. Therefore, the 30 MGPC scaffolds exhibited obvious degradation than 15 MGPC and GPC scaffolds. However, PCL scaffold showed no obvious degradation.

Figure 3E reveals the weight loss (degradation) of the scaffolds after immersed in Tris–HCl solution for different times. The weight loss of the scaffolds increased with time, indicating the scaffolds could be degradable. Moreover, the addition of GA into PCL obviously improved the degradation rate of GPC (GPC> PCL). Furthermore, the degradation rate of scaffolds increased with the increase of mMCS content (30 MGPC>15 MGPC> GPC).

Cell response to scaffolds
Cell attachment

Figure 4 shows the attachment ratio of the MC3T3-E1 cells on 30 MGPC, 15 MGPC, and GPC scaffolds at different times. The attachment ratio of the cells increased not only with time but also with mMCS content in the scaffolds. At 6 hours, no obvious differences of the cell attachment ratio for 30 MGPC, 15 MGPC, and GPC scaffolds were found. However, at both 12 and 24 hours, the attachment ratio of the cells on 30 MGPC was obviously higher than 15 MGPC scaffolds, and 15 MGPC was obviously higher than GPC scaffold.
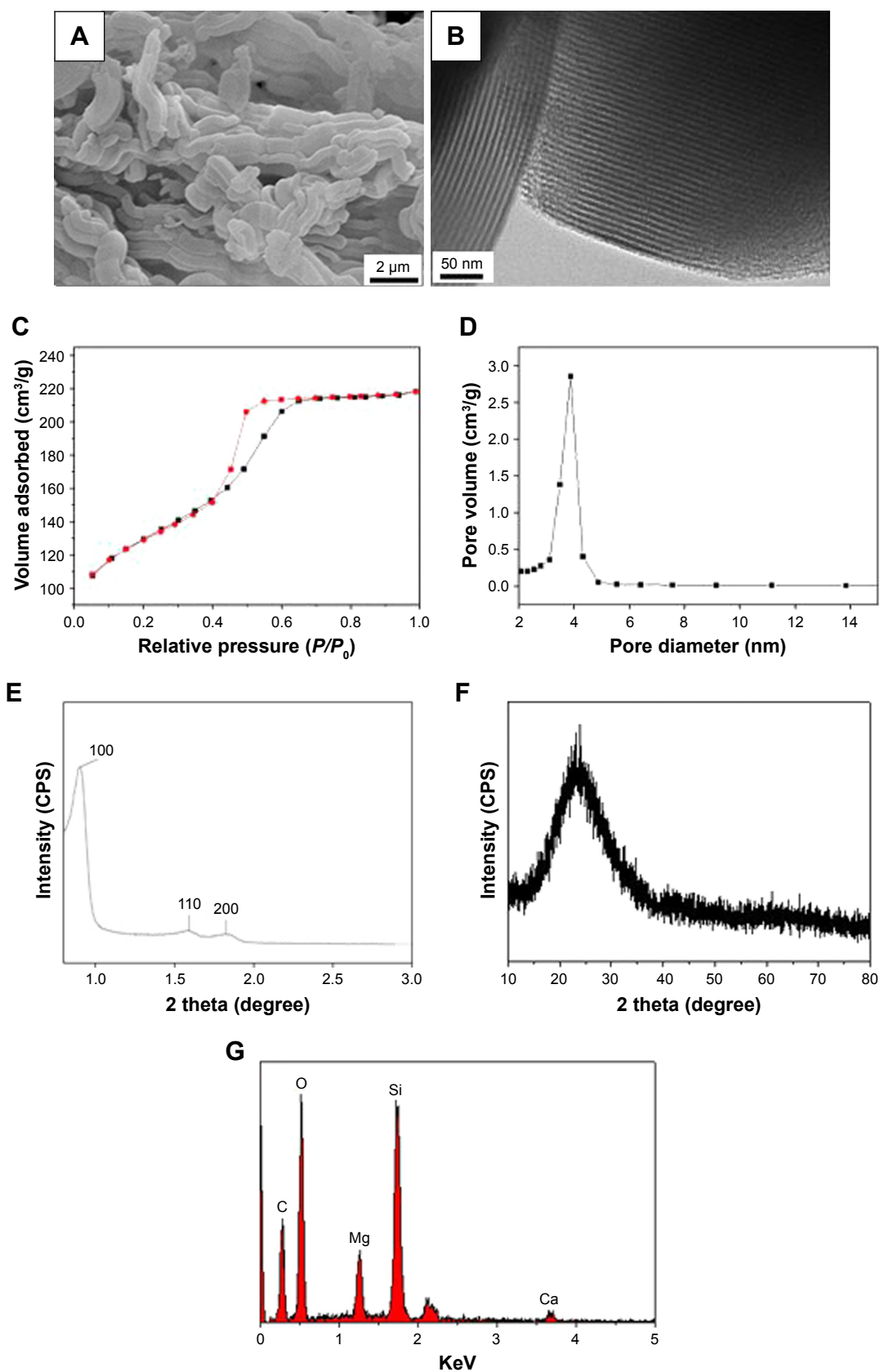
Figure 1 SEM (**A**) and TEM (**B**) micrographs of surface morphology of mMCS fibers; N$_2$ adsorption–desorption isotherms (**C**) and pore size distribution (**D**) of mMCS; small angle (**E**), wide angle (**F**) XRD, and EDS (**G**) of mMCS.
Notes: The magnification of figure **A** is ×12000; the magnification of figure **B** is ×400000.
Abbreviations: EDS, energy dispersive spectrometry; mMCS, mesoporous magnesium calcium silicate; SEM, scanning electron microscopy; TEM, transmission electron microscopy; XRD, X-ray diffraction.

Table 2 Porosity and compressive strength of 3D-printed scaffolds

Scaffolds samples	Porosity (%)	Compressive strength (MPa)
PCL	79.3±5.1	8.6±2.0
GPC	78.1±7.5	8.4±2.6
15 MGPC	77.6±5.4	10.5±2.3
30 MGPC	78.4±6.2	12.1±2.1

Abbreviations: GA, gliadin; MGPC, mMCS/GA/PCL composites; mMCS, mesoporous magnesium calcium silicate; PCL, polycaprolactone.

Figure 5 shows the SEM micrographs of the morphology of MC3T3-E1 cells cultivated on 30 MGPC, 15 MGPC, and GPC scaffolds for different times. At both 12 and 24 hours, the MC3T3-E1 cells with normal morphology attached and spread better on 30 MGPC surfaces than on 15 MGPC and GPC scaffolds, and 15 MGPC was better than GPC scaffold. Moreover, the amounts of attached cells on the scaffolds increased with time and mMCS content (30 MGPC>15 MGPC> GPC).

Cell proliferation

Figure 6 shows the optical density (OD) values of MC3T3-E1 cells (cells proliferation) cultivated on 30 MGPC, 15 MGPC, and GPC scaffolds at different times. It is found that the OD values for all the samples increased with time, indicating good cytocompatibility. At Day 1, there was no apparent difference in OD value for all the three kinds of samples. At Days 3 and 5, the OD value for 30 MGPC was obviously higher than 15 MGPC, and 15
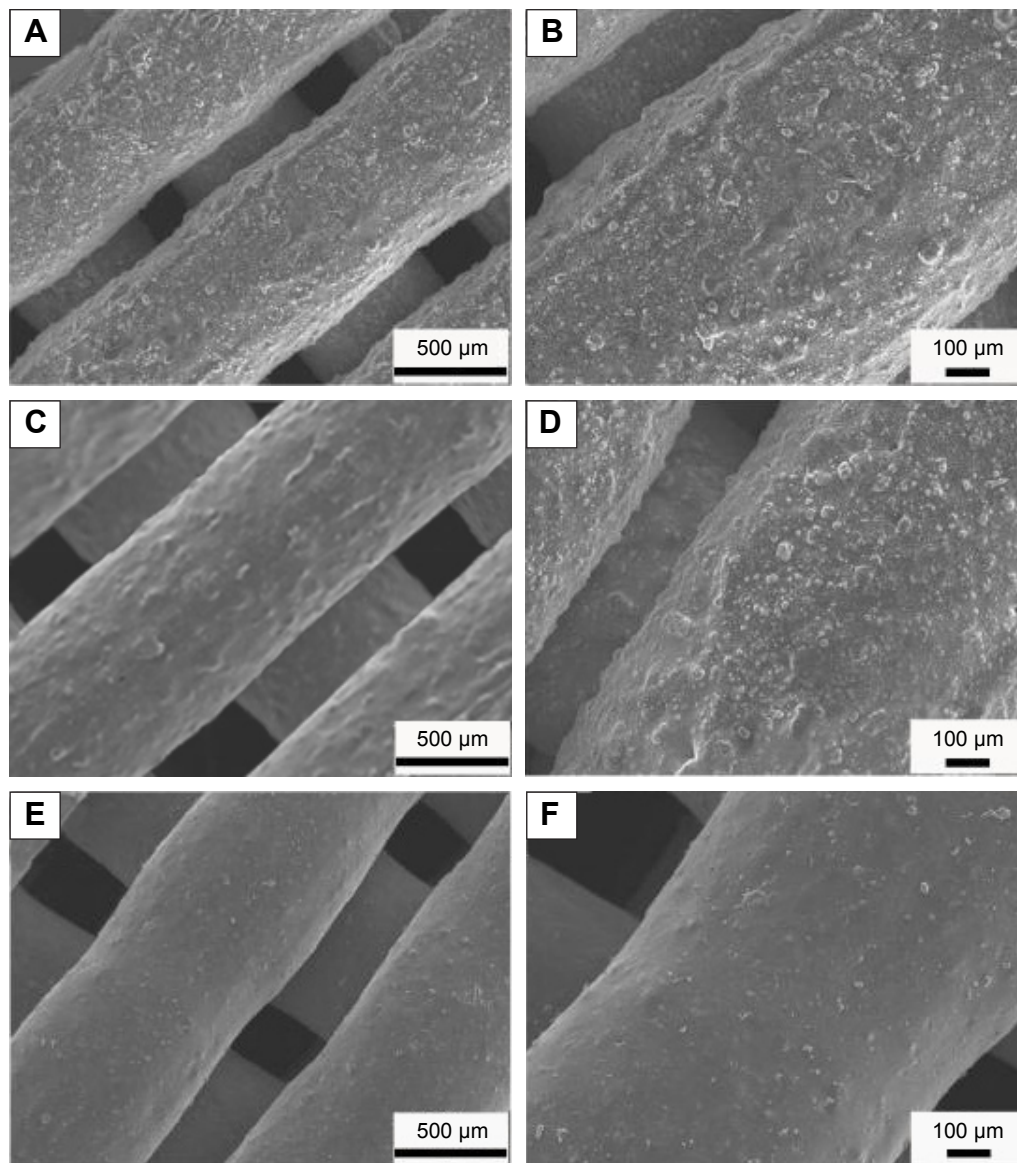

Figure 2 SEM micrographs of 30 MGPC (**A**, **B**), 15 MGPC (**C**, **D**) and GPC (**E**, **F**) scaffolds.
Notes: The magnification of figures **A**, **C**, and **E** is ×50; the magnification of figures **B**, **D**, and **F** is ×500.
Abbreviations: GA, gliadin; MGPC, mMCS/GA/PCL composites; mMCS, mesoporous magnesium calcium silicate; PCL, polycaprolactone.
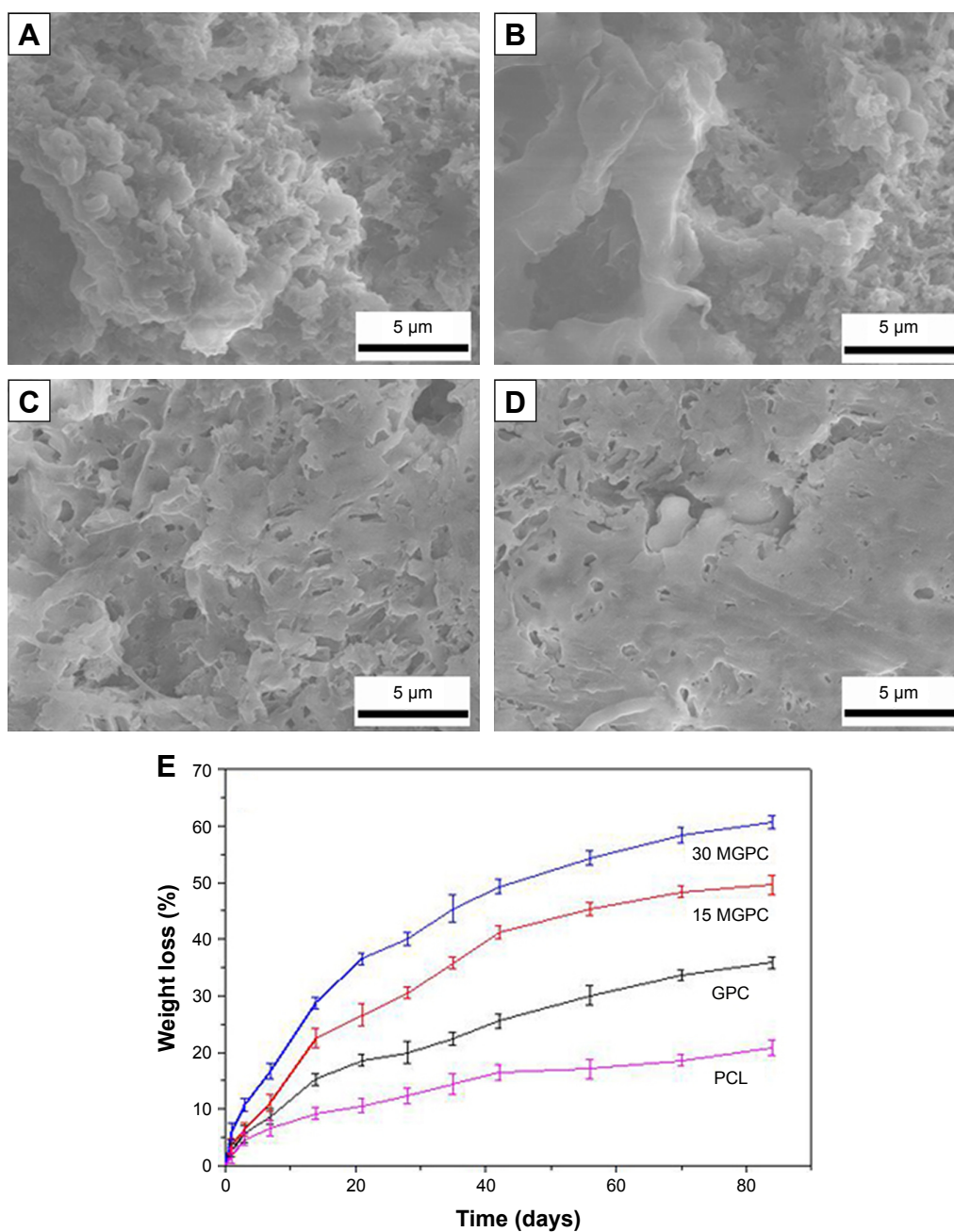
Figure 3 SEM micrographs of surface morphology of 30 MGPC (**A**), 15 MGPC (**B**), GPC (**C**), and PCL (**D**) scaffolds after immersed in Tris–HCl solution for 2 weeks, and change of weight loss (**E**) of the scaffolds immersed in Tris–HCl solution with time.
Note: The magnification of **A**–**D** is ×5000.
Abbreviations: GA, gliadin; MGPC, mMCS/GA/PCL composite; mMCS, mesoporous magnesium calcium silicate; PCL, polycaprolactone; SEM, scanning electron microscopy.

MGPC was higher than GPC scaffold. The results indicated that the 30 MGPC scaffold significantly promoted cells proliferation.

Scaffolds implanted into femoral defects of rabbits

Macro-observation

Figure 7 shows that photos of bone samples after 30 MGPC, 15 MGPC, and GPC scaffolds implanted in vivo for different times. No inflammation was observed during the postoperative follow-up, and the scaffolds caused no significant harm to the neighboring tissues. After 3 months postoperatively, the defects were completely repaired by 30 MGPC scaffold while the defects were not completely repaired by GPC scaffold.

Histological analysis

Figure 8A shows the images of histological sections of H&E staining after 30 MGPC, 15 MGPC, and GPC scaffolds implanted in vivo for different times. The results demonstrated
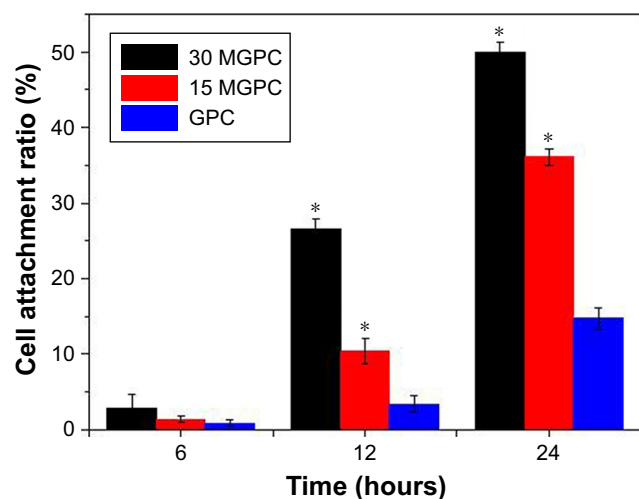
Figure 4 Attachment ratio of MC3T3-E1 cells on 30 MGPC, 15 MGPC, and GPC scaffolds at 6, 12, and 24 hours, *$P<0.05$.
Abbreviation: MGPC, mMCS/GA/PCL composite.

that the ossification in the scaffolds occurred as the degradation of the material during bone defect healing. The new bones (NBs) tissues were found to grow into both 30 MGPC and 15 MGPC scaffolds, which increased with time. However, only a few NBs were found in GPC scaffold at 3 months. Moreover, at 1, 2, and 3 months, significantly higher amounts of NBs were found within defects filled with 30 MGPC, compared with defects filled with 15 MGPC and GPC.

Figure 8B shows the quantitative analysis of the percentage of NBs area after the scaffolds were implanted in vivo for different times. The amount of NBs in all scaffolds increased with time, and the NBs in 30 MGPC scaffold were the highest among them (30 MGPC>15 MGPC> GPC) at 1, 2, and 3 months. Figure 8C shows the percentage of MR after the scaffolds were implanted in vivo for different

times. The amount of MRs in all scaffolds decreased with time, and the MRs for 30 MGPC scaffold were the lowest among (30 MGPC<15 MGPC< GPC) them at 2 and 3 months.

Immunohistochemical analysis

Figure 9A shows the images of immunohistological staining of type I collagen expression after the scaffolds were implanted in vivo for different times. The staining area of type I collagen expression for all scaffolds increased with time. At 1, 2, and 3 months, a significantly more staining area of type I collagen expression was observed in 30 MGPC than those in 15 MGPC and GPC scaffolds, and 15 MGPC was more than GPC scaffold. Figure 9B reveals the quantitative analysis of the type I collagen expression. It was found that the expression of type I collagen increased with time in all scaffolds. Moreover, at 2 and 3 months, the expression of type I collagen in 30 MGPC was obviously higher than 15 MGPC, and 15 MGPC was higher than GPC scaffold. These results indicated that the bone formation was most actively progressing in 30 MGPC scaffold.

Discussion

To facilitate desired bone tissue regeneration, the structural design of the scaffold often considers factors such as porosity, pore size and morphology, and pore interconnectivity.[18] The main disadvantage of the scaffolds prepared by traditional methods (solvent casting and particulate-leaching, freeze-drying, phase separation, etc.) is the uncontrollable architecture (eg, pores are not uniform and interconnective), which might be compromised for efficient cell/tissue ingrowth and
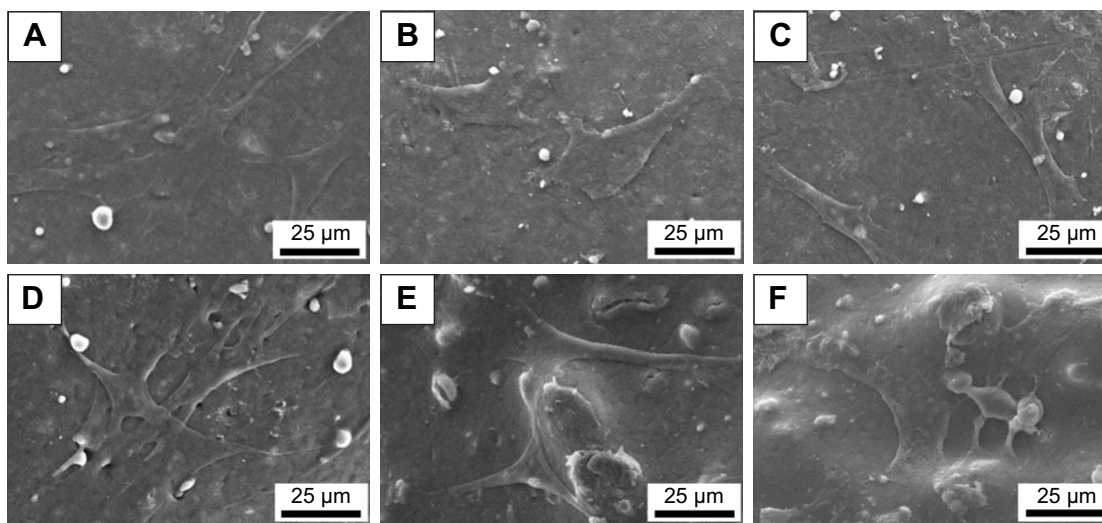

Figure 5 SEM micrographs of MC3T3-E1 cells cultured on 30 MGPC (**A**, **D**), 15 MGPC (**B**, **E**), and GPC (**C**, **F**) scaffolds for 12 (**A**, **B**, **C**) and 24 hours (**D**, **E**, **F**).
Note: The magnification of the figures is ×800.
Abbreviations: GA, gliadin; MGPC, mMCS/GA/PCL composites; mMCS, mesoporous magnesium calcium silicate; PCL, polycaprolactone.
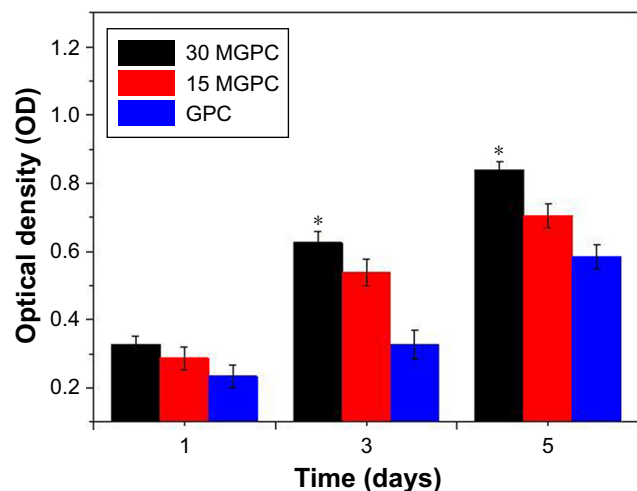
Figure 6 Change of OD values of MC3T3-E1 cells on 30 MGPC, 15 MGPC, and GPC scaffolds with time, *$P<0.05$.
Abbreviations: GA, gliadin; MGPC, mMCS/GA/PCL composites; mMCS, mesoporous magnesium calcium silicate; PCL, polycaprolactone.

nutrient transport.[19,20] Therefore, in this study, the ternary composite scaffolds containing mMCS fibers, GA, and PCL were fabricated by 3D-printing technology.

The results showed that the porous structure (including porosity, pore size, pore morphology, and pore interconnectivity) of the 3D-printed scaffolds (30 MGPC, 15 MGPC, and GPC) could be efficiently adjusted. The 3D-printed scaffolds possessed well interconnected macropores with the pores sizes of about 300 µm and porosity of 78%. Moreover, both 30 MGPC and 15 MGPC scaffolds exhibited rough surfaces while GPC showed smooth surface. The formations of rough surfaces of both 30 MGPC and 15 MGPC scaffolds were due to the presence of mMCS, which were exposed on the scaffolds surfaces. In addition, the compressive strengths of 30 MGPC, 15 MGPC, and GPC scaffolds were 12.1, 10.5, and 8.4 MPa, respectively, indicating that
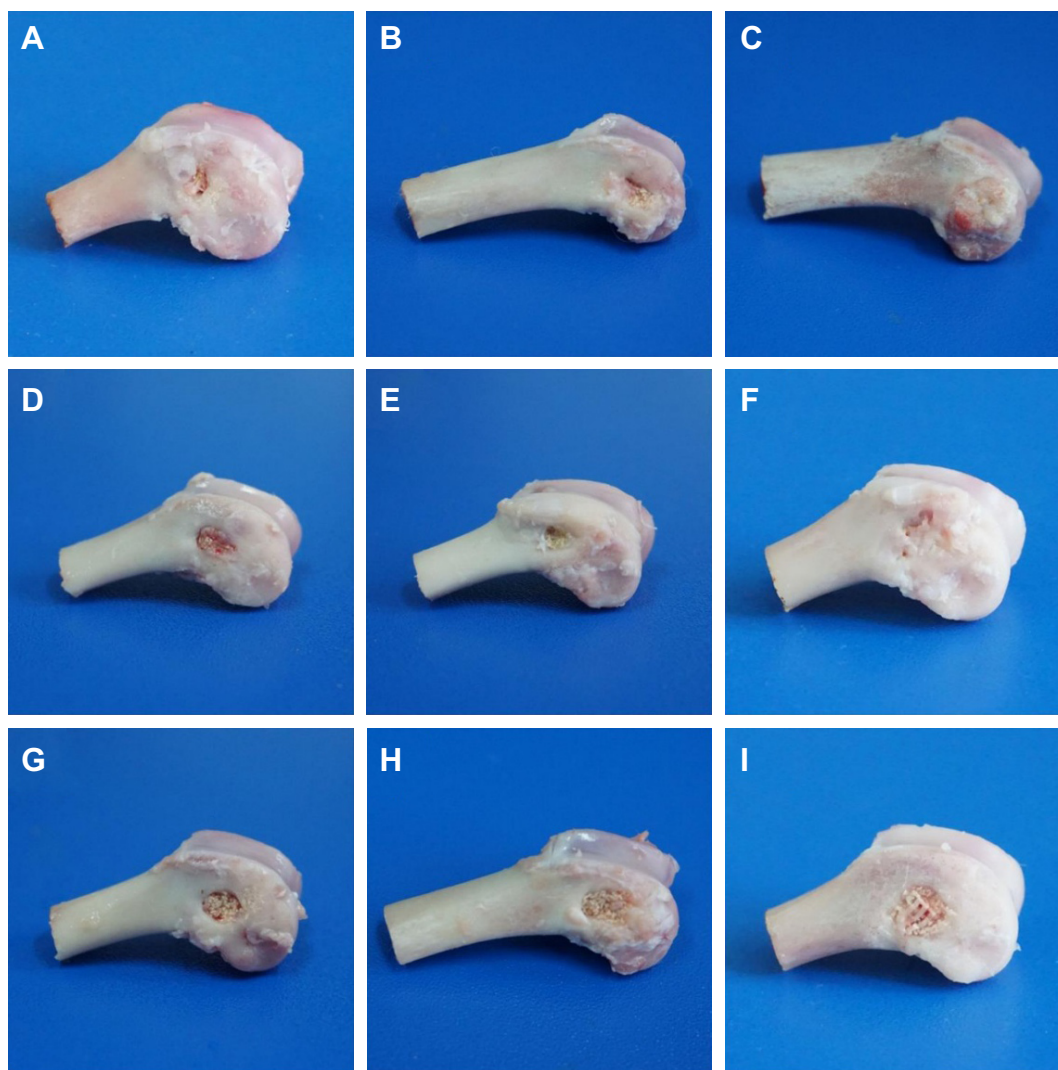

Figure 7 Photos of bone after 30 MGPC (**A–C**), 15 MGPC (**D–F**), and GPC (**G–I**) scaffolds implanted into femoral defects for 1 (**A**, **D**, **G**), 2 (**B**, **E**, **H**) and 3 months (**C**, **F**, **I**).
Abbreviations: GA, gliadin; MGPC, mMCS/GA/PCL composites; mMCS, mesoporous magnesium calcium silicate; PCL, polycaprolactone.
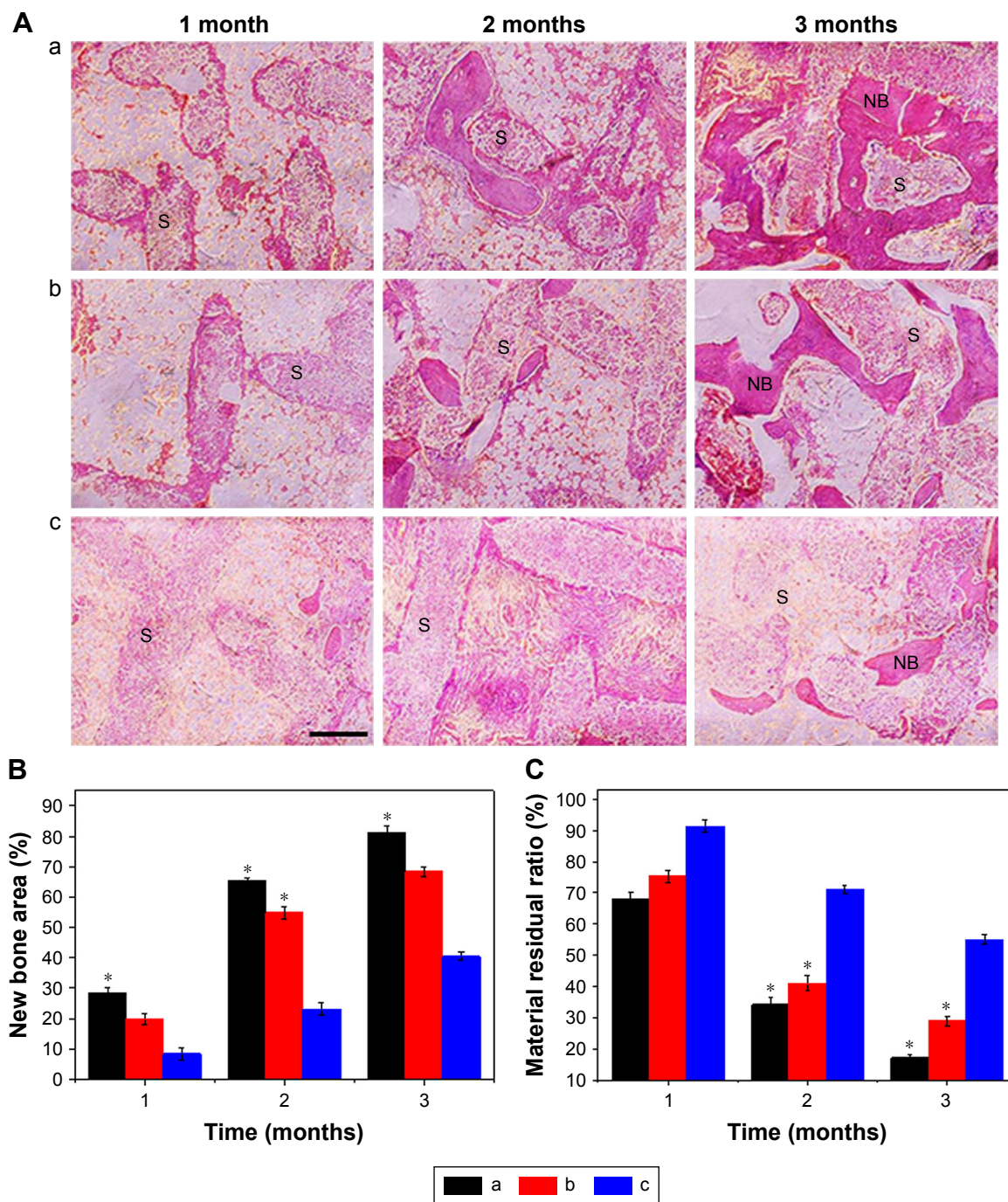
Figure 8 The images (**A**) of histological sections of H&E staining after 30 MGPC (a), 15 MGPC (b), and GPC (c) scaffolds implanted into femoral defects of rabbits for 1, 2, and 3 months. Scale bar: 200 μm. Percentage of newly formed bone area (**B**) and material residual (**C**) after 30 MGPC (a), 15 MGPC (b), and GPC (c) scaffolds implanted in vivo for 1, 2, and 3 months, *$P<0.05$.
Note: The magnification of figure **A** is ×200.
Abbreviations: GA, gliadin; MGPC, mMCS/GA/PCL composites; mMCS, mesoporous magnesium calcium silicate; NB, new bone; PCL, polycaprolactone; S, scaffolds.

the compressive strengths of the scaffolds increased with the increase of mMCS content (30 MGPC>15 MGPC> GPC) due to the reinforcement of mMCS fibers in the polymer matrix. The compressive strength of 30 MGPC scaffolds of 12.1 MPa was higher than that of cancellous bone, which is in the range of 3–15 MPa.[21]

Ideal scaffolds for bone regeneration should be desirable to possess the matched speed of degradation with the formation of NBs when implanted in vivo.[22] In this study, the results showed that the degradation rate of 30 MGPC was obviously faster than 15 MGPC, and 15 MGPC was faster than GPC scaffold. It could be suggested that the incorporation of
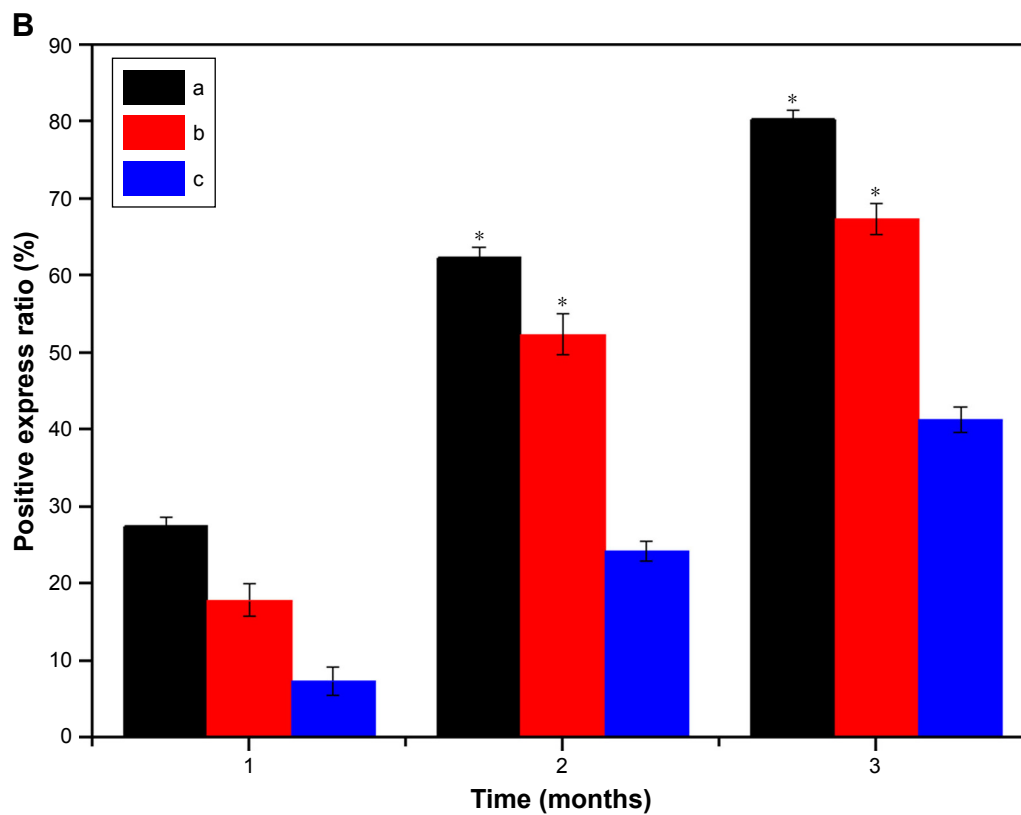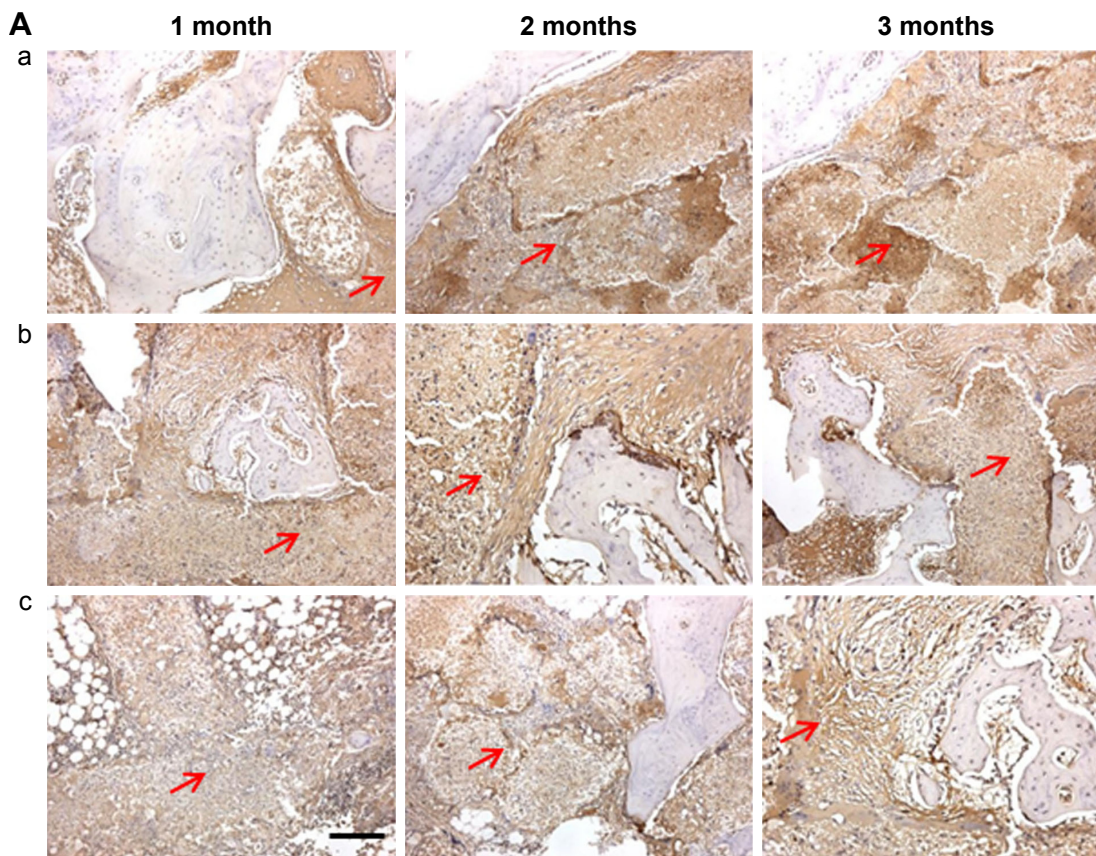
Figure 9 Images (**A**) of immunohistological staining of type I collagen expression (brown: arrows, scale bar: 200 μm), and quantitative analysis of type I collagen expression (**B**) after 30 MGPC (a), 15 MGPC (b), and GPC (c) scaffolds were implanted into femoral defects of rabbits for 1, 2, and 3 months, *P<0.05.
Note: The magnification of Figure **A** is ×200.
Abbreviations: GA, gliadin; MGPC, mMCS/GA/PCL composites; mMCS, mesoporous magnesium calcium silicate; PCL, polycaprolactone.

mMCS fibers with large surface area and high pore volume (enhanced dissolution) was conducive to improve the degradability of the scaffolds, which increased with the increase of mMCS content, in which the 30 MGPC scaffold possessed the fastest degradation rate among them. Moreover, the degradation rate of GPC was faster than PCL scaffold, indicating that addition of GA into PCL would improve the degradability of the GPC scaffolds (degradation rate of PCL is very slow). Obviously, the presence of GA also enhanced the degradability of the 30 MGPC and 15 MGPC scaffolds.

The first stage of cell biological responses to a scaffold is attachment, which depends on the surface characteristics (including surface topography and chemistry) of the scaffold, and the attachment and spreading of cells on scaffold surface may further regulate cellular behaviors and functions (eg, proliferation and differentiation).[23] In this study, the attachment ratio of MC3T3-E1 cells on 30 MGPC was obviously higher than 15 MGPC scaffolds, and 15 MGPC was higher than GPC scaffold. Moreover, the SEM images showed that the cells with normal morphology attached and spread better on the surface of 30 MGPC than 15 MGPC, and better on 15 MGPC than GPC, revealing that the 30 MGPC with high mMCS content was beneficial to the cells attachment and growth, indicating good cytocompatibility. Previous reports have shown that the rough surface of the scaffold could be helpful to boost the interactions between the substrates and cells, and then contributed to cell attachment and growth.[24] Therefore, the mechanism of the scaffolds promoting cells attachment might contain two factors: one was rough surface, which was caused by mMCS on scaffolds surfaces (surface topography) and the other was mMCS particles with bioactivity on scaffolds surfaces (surface chemistry). It can be suggested that the synergistic effect of the rough surface of scaffolds and bioactivity of mMCS on scaffolds promoted the cells attachment and growth.

Generally, the level of cells proliferation can be expressed by the optical density (OD) values, and ideal scaffolds should promote the cell proliferation.[25] In this study, the OD value of the MC3T3-E1 cells for 30 MGPC was significantly higher than 15 MGPC, and 15 MGPC was higher than GPC scaffold, indicating that the increase of mMCS content in the scaffolds promoted the cells proliferation. Therefore, it can be suggested that the effective promotion of the cells proliferation and growth into scaffolds were attributed to the presence of bioactive mMCS on the surfaces of the scaffolds. The results indicated that the 30 MGPC scaffold could support the attachment, growth, and proliferation of MC3T3-E1 cells, indicating excellent cytocompatibility. Some studies have shown that ionic products (eg, Si, Ca, and Mg) dissolution from bioglass/bioceramics could stimulate osteoblasts proliferation and differentiation.[26] In this study, the 30 MGPC scaffold could be degradable, and the continuous dissolution of 30 MGPC scaffold containing mMCS might produce a microenvironment containing Si, Ca, and Mg ions.[27] Therefore, it can be suggested that the enhancement of the cells responses (such as growth and proliferation) might be ascribed to the release of Si, Ca, and Mg ions from the degradation of 30 MGPC scaffold.

After the scaffolds were implanted in vivo for different times, the scaffolds caused no inflammation and no significant harm to their neighboring tissues, showing good biocompatibility. At each time point, the bone regeneration ability within defects was evaluated by histological sections, which revealed the progression of bone formation efficacy. The results revealed more NBs in 30 MGPC than in 15 MGPC and GPC scaffolds at 1, 2, and 3 months post implantation. Therefore, it could be suggested that the 30 MGPC significantly stimulated effective osteogenesis compared with 15 MGPC and GPC scaffolds. Quantitative comparison of the percentage of new bone area also revealed significant osteogenesis in 30 MGPC scaffold than in 15 MGPC and GPC at 1, 2, and 3 months. Therefore, the results suggested that the bone regeneration ability of the scaffolds significantly enhanced with the increase of mMCS content, in which the 30 MGPC scaffold possessed the best osteogenesis.

The amounts of MRs for all scaffolds decreased with time, indicating good degradability in vivo. Moreover, the amounts of MRs for 30 MGPC scaffold were obviously lower than 15 MGPC and GPC at 1, 2, and 3 months, indicating that 30 MGPC scaffold possessed fastest degradation rate among all scaffolds in vivo. It can be suggested that the improvement of the degradability of 30 MGPC was due to the high content of mMCS in the scaffolds. Therefore, the results demonstrated that the ossification occurred as the degradation of the material during defect healing. It is known that the dissolution of a scaffold can be considered as degradation in vitro while the dissolution and cell-mediated degradation were two main factors that affected the degradation of the scaffold in vivo.[28,29] Furthermore, the results revealed that the degradation of the scaffolds in vivo was faster than in vitro. Therefore, the results indicated that the in vivo degradation of the scaffolds was controlled by both the dissolution and cell-mediated degradation.

Type I collagen is a major component of bone matrix proteins, which was secreted at the early phase of osteoid matrix deposition and modulated cell differentiation, and the expression of collagen I was a nonspecific marker of new bone formation.[30] In this study, the results of type I

collagen staining and quantitative analysis of type I collagen expression revealed that the expression of type I collagen for 30 MGPC was significantly higher than 15 MGPC, and 15 MGPC was higher than GPC scaffold, indicating that 30 MGPC promoted remarkable new bone formation compared with 15 MGPC and GPC scaffolds. Therefore, the immunohistochemical analysis of type I collagen further offered the direct evidence of the stimulatory effect on cells osteogenic differentiation and osteoid matrix deposition in vivo with the help of 30 MGPC scaffold.

There were two potential reasons to explain why 30 MGPC possessed the improved osteogenesis in vivo compared with 15 MGPC and GPC scaffolds. One was that the 30 MGPC scaffold did have a quicker degradation rate than 15 MGPC and GPC. The fast degradation of 30 MGPC in vivo might provide a proper room for matrix deposition and new bone ingrowth. However, GPC with a slower degradation rate might influence the in vivo new bone ingrowth. Another was the faster release of Si, Ca, and Mg ions from 30 MGPC scaffold (faster degradation) than 15 MGPC (30 MGPC releases more ions than 15 MGPC) in vivo. Previous studies have shown that the Si, Ca, and Mg ionic products from bioglass/ceramics significantly stimulated the proliferation and differentiation, and promoted new bone formation in vivo.[31,32] Therefore, it is reasonable to speculate that in the current study, the release of these ionic products from 30 MGPC might promote the functions of osteoblasts in vivo and enhanced the osteogenesis. Furthermore, the study indicated that both mMCS and GA in 30 MGPC scaffolds played important roles to regulate the in vivo osteogenesis and the degradation of the scaffolds (GPC> PCL). In short, the 30 MGPC scaffold incorporated with mMCS and GA could significantly not only upregulate cells responses in vitro but also promoted osteogenesis in vivo. Therefore, the 30 MGPC scaffold might have a great potential for application in tissue engineering.

Conclusion

In this study, the bioactive 30 MGPC scaffold of mMCS/ GA/PCL ternary composite was prepared by 3D-printing technology, and the porous structure of the 3D-printed scaffolds could be efficiently adjusted. The results demonstrated that the introduction of mMCS and GA into PCL led to the improvement of the compressive strength and in vitro degradability of the 3D-printed scaffolds, which depended on the mMCS content. In addition, compared with 15 MGPC and GPC scaffolds, the 30 MGPC scaffold with high mMCS content obviously promoted cell adhesion, growth, and proliferation, indicating good cytocompatibility. The 3D-printed

30 MGPC obviously promoted new bone formation and growth into the scaffold compared with 15 MGPC and GPC scaffolds, indicating that the 30 MGPC scaffolds significantly improved osteogenesis through materials degradation in vivo. The 30 MGPC scaffold with good biocompatibility, compressive strength, degradability, and excellent in vivo osteogenesis had a great potential for application in tissue engineering.

Disclosure

The authors report no conflicts of interest in this work.

References

1. Seyednejad H, Gawlitta D, Kuiper RV, et al. In vivo biocompatibility and biodegradation of 3D-printed porous scaffolds based on a hydroxyl-functionalized poly(ε-caprolactone). *Biomaterials*. 2012;33(17): 4309–4318.
2. Wang Y, Kim UJ, Blasioli DJ, Kim HJ, Kaplan DL. In vitro cartilage tissue engineering with 3D porous aqueous-derived silk scaffolds and mesenchymal stem cells. *Biomaterials*. 2005;26(34):7082–7094.
3. Zhou C, Shi Q, Guo W, et al. Electrospun bio-nanocomposite scaffolds for bone tissue engineering by cellulose nanocrystals reinforcing maleic anhydride grafted PLA. *ACS Appl Mater Interfaces*. 2013; 5(9):3847–3854.
4. Miguez-Pacheco V, Hench LL, Boccaccini AR. Bioactive glasses beyond bone and teeth: emerging applications in contact with soft tissues. *Acta Biomater*. 2015;13:1–15.
5. Liu Y, Lim J, Teoh SH. Review: development of clinically relevant scaffolds for vascularised bone tissue engineering. *Biotechnol Adv*. 2013; 31(5):688–705.
6. Nair BP, Gangadharan D, Mohan N, Sumathi B, Nair PD. Hybrid scaffold bearing polymer-siloxane Schiff base linkage for bone tissue engineering. *Mater Sci Eng C Mater Biol Appl*. 2015;52: 333–342.
7. Torabinejad B, Mohammadi-Rovshandeh J, Davachi SM, Zamanian A. Synthesis and characterization of nanocomposite scaffolds based on triblock copolymer of L-lactide, ε-caprolactone and nano-hydroxyapatite for bone tissue engineering. *Mater Sci Eng C Mater Biol Appl*. 2014;42:199–210.
8. Saber-Samandari S, Saber-Samandari S, Kiyazar S, Aghazadeh J, Sadeghi A. In vitro evaluation for apatite-forming ability of cellulose-based nanocomposite scaffolds for bone tissue engineering. *Int J Biol Macromol*. 2016;86:434–442.
9. Ct W, Fan W, Zhou YH, et al. 3D-printing of highly uniform CaSiO3 ceramic scaffolds: preparation, characterization and in vivo osteogenesis. *J Mater Chem*. 2012;22:12288–12295.
10. Bracaglia LG, Smith BT, Watson E, Arumugasaamy N, Mikos AG, Fisher JP. 3D printing for the design and fabrication of polymer-based gradient scaffolds. *Acta Biomater*. 2017;56:3–13.

11. de Valence S, Tille JC, Mugnai D, et al. Long term performance of polycaprolactone vascular grafts in a rat abdominal aorta replacement model. *Biomaterials*. 2012;33(1):38–47.

12. Ji L, Wang W, Jin D, Zhou S, Song X. In vitro bioactivity and mechanical properties of bioactive glass nanoparticles/polycaprolactone composites. *Mater Sci Eng C Mater Biol Appl*. 2015;46:1–9.

13. Reddy N, Yang Y. Potential of plant proteins for medical applications. *Trends Biotechnol*. 2011;29(10):490–498.

14. Reddy N, Yang Y. Self-crosslinked gliadin fibers with high strength and water stability for potential medical applications. *J Mater Sci Mater Med*. 2008;19(5):2055–2061.

15. Vaid C, Murugavel S. Alkali oxide containing mesoporous bioactive glasses: synthesis, characterization and in vitro bioactivity. *Mater Sci Eng C Mater Biol Appl*. 2013;33(2):959–968.

16. Ding Y, Tang S, Yu B, et al. In vitro degradability, bioactivity and primary cell responses to bone cements containing mesoporous magnesium-calcium silicate and calcium sulfate for bone regeneration. *J R Soc Interface*. 2015;12(111):20150079.

17. Wu Y, Tang X, Chen J, et al. Improvement of bioactivity, degradability, and cytocompatibility of biocement by addition of mesoporous magnesium silicate into sodium-magnesium phosphate cement. *J Mater Sci Mater Med*. 2015;26(9):1–10.

18. Ashworth JC, Mehr M, Buxton PG, Best SM, Cameron RE. Cell invasion in collagen scaffold architectures characterized by percolation theory. *Adv Health Mater*. 2015;4(9):1317–1321.

19. Peng X-F, Mi H-Y, Jing X, et al. Preparation of highly porous interconnected poly(lactic acid) scaffolds based on a novel dynamic elongational flow procedure. *Mater Des*. 2016;101:285–293.

20. Wg L, Jang J, Kim BS, Lee MS, Cho DW, Yang HS. Systemically replicated organic and inorganic bony microenvironment for new bone formation generated by a 3D printing technology. *RSC Advances*. 2016;6:11546–11553.

21. Roohani-Esfahani SI, Newman P, Zreiqat H. Design and fabrication of 3D printed scaffolds with a mechanical strength comparable to cortical bone to repair large bone defects. *Sci Rep*. 2016;6:19468.

22. Pina S, Oliveira JM, Reis RL. Natural-based nanocomposites for bone tissue engineering and regenerative medicine: a review. *Adv Mater*. 2015;27(7):1143–1169.

23. Liu X, Feng Q, Bachhuka A, Vasilev K. Surface modification by allylamine plasma polymerization promotes osteogenic differentiation of human adipose-derived stem cells. *ACS Appl Mater Interfaces*. 2014;6(12):9733–9741.

24. Balasundaram G, Storey DM, Webster TJ. Novel nano-rough polymers for cartilage tissue engineering. *Int J Nanomed*. 2014;9:1845–1853.

25. Liu H, Peng H, Wu Y, et al. The promotion of bone regeneration by nanofibrous hydroxyapatite/chitosan scaffolds by effects on integrin-BMP/Smad signaling pathway in BMSCs. *Biomaterials*. 2013;34(18):4404–4417.

26. Mladenović Ž, Johansson A, Willman B, Shahabi K, Björn E, Ransjö M. Soluble silica inhibits osteoclast formation and bone resorption in vitro. *Acta Biomater*. 2014;10(1):406–418.

27. Chen S, Yang Q, Brow RK, et al. In vitro stimulation of vascular endothelial growth factor by borate-based glass fibers under dynamic flow conditions. *Mater Sci Eng C Mater Biol Appl*. 2017;73:447–455.

28. Cunniffe GM, Vinardell T, Thompson EM, et al. Chondrogenically primed mesenchymal stem cell-seeded alginate hydrogels promote early bone formation in critically-sized defects. *Eur Polym J*. 2015;72:464–472.

29. Kerpes R, Fischer S, Becker T. The production of gluten-free beer: degradation of hordeins during malting and brewing and the application of modern process technology focusing on endogenous malt peptidases. *Trends Food Sci Technol*. 2017;67:129–138.

30. Shrestha S, Mao Z, Fedutik Y, Gao C. Influence of titanium dioxide nanorods with different surface chemistry on the differentiation of rat bone marrow mesenchymal stem cells. *J Mater Chem B*. 2016;4(43):6955–6966.

31. Montazerian M, Yekta BE, Marghussian VK, Bellani CF, Siqueira RL, Zanotto ED. Bioactivity and cell proliferation in radiopaque gel-derived $CaO-P_2O_5-SiO_2-ZrO_2$ glass and glass-ceramic powders. *Mater Sci Eng C Mater Biol Appl*. 2015;55:436–447.

32. Zhang M, Chen X, Pu X, Liao X, Huang Z, Yin G. Different effects of a novel $CaO-MgO-SiO_2$-based multiphase glass-ceramic on cell behaviors of normal and cancer cells in vitro. *Colloids Surf B Biointerfaces*. 2014;116:1–8.